

Diffraction and its QCD interpretation

Laurent SCHOEFFEL¹

(1) CEA Saclay/Irfu-SPP, 91191 Gif-sur-Yvette, France

Abstract

The most important results on hadronic diffractive phenomena obtained at HERA and Tevatron are reviewed and new issues in nucleon tomography are discussed. Some challenges for understanding diffraction at the LHC, including the discovering of the Higgs boson, are outlined.

1. Experimental diffraction at HERA

Between 1992 and 2007, the HERA accelerator provided ep collisions at center of mass energies beyond 300 GeV at the interaction points of the H1 and ZEUS experiments. Perhaps the most interesting results to emerge relate to the newly accessed field of perturbative strong interaction physics at low Bjorken- x (x_{Bj}), where parton densities become extremely large. Questions arise as to how and where non-linear dynamics tame the parton density growth and challenging features are observed. Central to this low x_{Bj} physics landscape is a high rate of diffractive processes, in which a colorless exchange takes place and the proton remains intact. Indeed, one of the most important experimental result from the DESY ep collider HERA is the observation of a significant fraction of events in Deep Inelastic Scattering (DIS) with a large rapidity gap (LRG) between the scattered proton, which remains intact, and the rest of the final system. This fraction corresponds to about 10% of the DIS data at $Q^2 = 10 \text{ GeV}^2$.

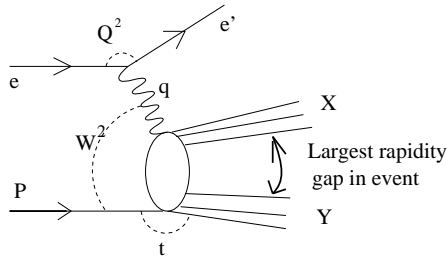


Fig. 1. Picture of the process $ep \rightarrow eXY$. The hadronic final state is composed of two distinct systems X and Y , which are separated by the largest interval in rapidity between final state hadrons.

In DIS, such events are not expected in such abundance, since large gaps are exponentially suppressed due to color string formation between the proton remnant and the scattered partons. Events are of the type $ep \rightarrow eXp$, where the final state proton carries more than 95 % of the proton beam energy. A photon of virtuality Q^2 , coupled to the electron (or positron), undergoes a strong interaction with the proton (or one of its low-mass excited states Y) to form a hadronic final state system X of mass M_X separated by a LRG from the leading proton (see Fig. 1.). These events are called diffractive. In such a reaction, $ep \rightarrow eXp$, no net quantum number is exchanged and the longitudinal momentum fraction $1 - x_P$ is lost by the proton. Thus, the longitudinal momentum $x_P P$ is transferred to the system X . In addition to the standard DIS kinematic variables and x_P , a diffractive event is also often characterized by the vari-

able $\beta = x_{Bj}/x_P$, which takes a simple interpretation in the parton model discussed in the following. Comparisons with hard diffraction in proton-(anti)proton scattering have also improved our knowledge of absorptive and underlying event effects in which the diffractive signature may be obscured by multiple interactions in the same event. In addition to their fundamental interest in their own right, these issues are highly relevant to the modeling of chromodynamics at the LHC.

Experimentally, for a diffractive DIS event, $ep \rightarrow eXp$, the dissociating particle is the virtual photon emitted by the electron. The final state consists of the scattered electron and hadrons which populate the photon fragmentation region. The proton is scattered in the direction of the initial beam proton with little change in momentum and angle. In particular, we detect no hadronic activity in the direction of the proton flight, as the proton remains intact in the diffractive process. On the contrary, for a standard DIS event, the proton is destroyed in the reaction and the flow of hadronic clusters is clearly visible in the proton fragmentation region (forward part of the detector).

The experimental selection of diffractive events in DIS proceeds in two steps. Events are first selected based on the presence of the scattered electron in the detector. Then, for the diffractive selection itself, three different methods have been used at HERA:

1. A reconstructed proton track is required in the leading (or forward) proton spectrometer (LPS for ZEUS or FPS for H1) with a fraction of the initial proton momentum $x_L > 0.97$. Indeed, the cleanest selection of diffractive events with photon dissociation is based on the presence of a leading proton in the final state. By leading proton we mean a proton which carries a large fraction of the initial beam proton momentum. This is the cleanest way to select diffractive events, but the disadvantage is a reduced kinematic coverage.
2. The hadronic system X measured in the central detector is required to be separated by a large rapidity gap from the rest of the hadronic final state. This is a very efficient way to select diffractive events in a large kinematic domain, close to the standard DIS one. The prejudice is a large background as discussed in the following.
3. The diffractive contribution is identified as the excess of events at small M_X above the exponential fall-off of the non-diffractive contribution with decreasing $\ln M_X^2$. The exponential fall-off, expected in QCD, permits the subtraction of the non-diffractive contribution and therefore the extraction of the diffractive contribution without assuming the precise M_X dependence of the latter. This is also a very efficient way to select diffractive events in a large kinematic domain.

Extensive measurements of diffractive DIS cross sections have been made by both the ZEUS and H1 collaborations at HERA, using different experimental techniques [1, 2]. Of course, the comparison of these techniques provides a

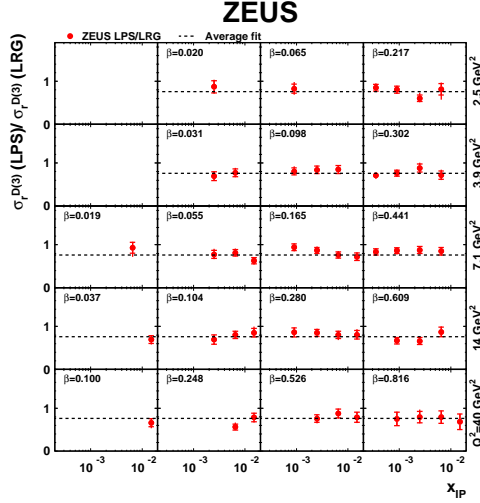


Fig. 2. Ratio of the diffractive cross sections, as obtained with the LPS and the LRG experimental techniques. The lines indicate the average value of the ratio, which is about 0.86. It implies that the LRG sample contains about 24% of proton dissociation events, corresponding to processes like $ep \rightarrow eXY$, where $M_Y < 2.3$ GeV. This fraction is approximately the same for H1 data (of course in the same M_Y range).

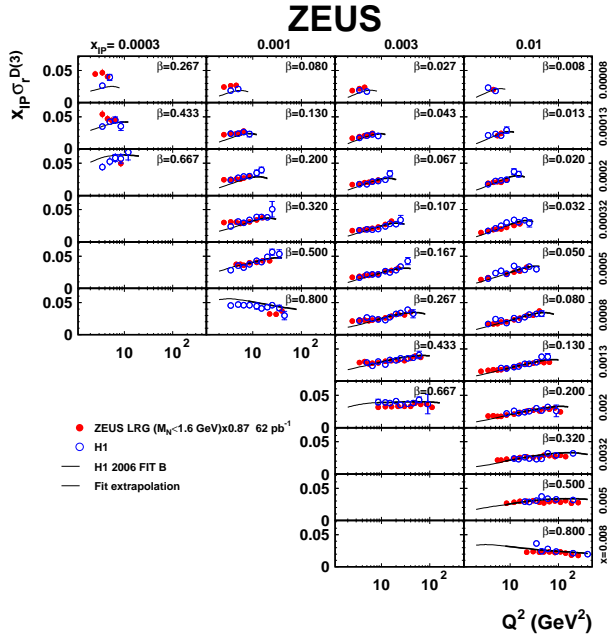


Fig. 3. The diffractive cross sections obtained with the LRG method by the H1 and ZEUS experiments. The ZEUS values have been rescaled (down) by a global factor of 13 %. This value is compatible with the normalisation uncertainty of this sample.

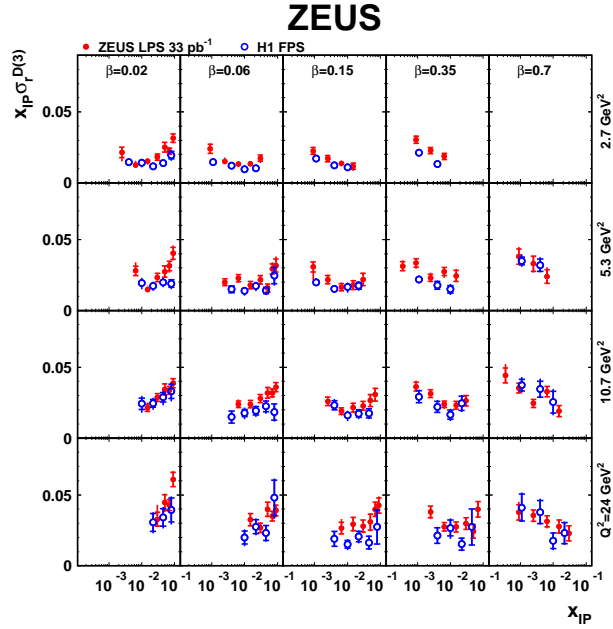


Fig. 4. The diffractive cross section obtained with the FPS (or LPS) method by the H1 and ZEUS experiments, where the proton is tagged. The ZEUS measurements are above H1 by a global factor of about 10%.

rich source of information to get a better understanding of the experimental gains and prejudices of those techniques. These last published set of data [2] contain five to seven times more statistics than in preceding publications of diffractive cross sections, and thus opens the way to new developments in data/models comparisons. A first relative control of the data samples is shown in Fig. 2., where the ratio of the diffractive cross sections is displayed, as obtained with the LPS and the LRG experimental techniques. The mean value of the ratio of 0.86 indicates that the LRG sample contains about 24% of proton-dissociation background, which is not present in the LPS sample. This background corresponds to events like $ep \rightarrow eXY$, where Y is a low-mass excited state of the proton (with $M_Y < 2.3$ GeV). It is obviously not present in the LPS analysis which can select specifically a proton in the final state. This is the main background in the LRG analysis. Due to a lack of knowledge of this background, it causes a large normalization uncertainty of 10 to 15 % for the cross sections extracted from the LRG analysis. We can then compare the results obtained by the H1 and ZEUS experiments for diffractive cross sections (in Fig. 3.), using the LRG method. A good compatibility of both data sets is observed, after rescaling the ZEUS points by a global factor of 13%. This factor is compatible with the normalization uncertainty described above. We can also compare the results obtained by the H1 and ZEUS experiments (in Fig. 4.), using the tagged proton method (LPS for ZEUS and FPS for H1). In this case, there is no proton dissociation background and the diffractive sample is expected to be clean. It gives a good reference to compare both experiments. A global normalization difference of about 10% can be observed in Fig. 4., which can be studied with more data. It remains compatible with the normalization uncertainty for this tagged proton sample. It is interesting to note that the ZEUS measurements are globally above the H1 data by about 10% for both tech-

niques, tagged proton or LRG. The important message at this level is not only the observation of differences as illustrated in Fig. 3. and 4., but the opportunity opened with the large statistics provided by the ZEUS measurements. Understanding discrepancies between data sets is part of the experimental challenge. It certainly needs analysis of new data sets from the H1 experiment. However, already at the present level, much can be done with existing data for the understanding of diffraction at HERA.

2. Soft physics at the proton vertex

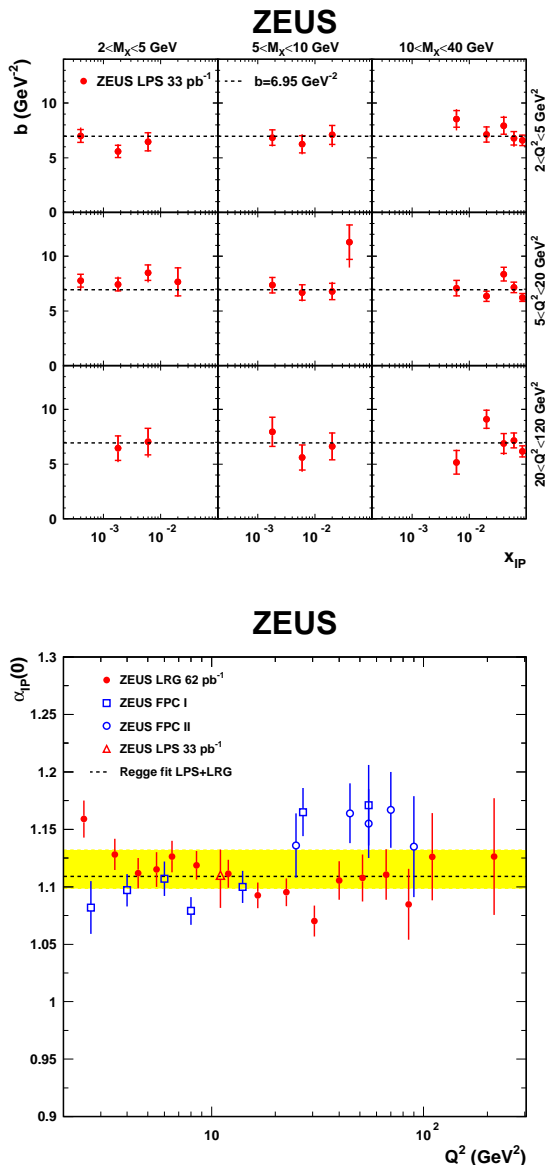


Fig. 5. (a) -top- Measurements of the exponential t slope from ZEUS LPS data, shown as a function of Q^2 , $x_{\mathbb{P}}$ and M_X . (b) -bottom- ZEUS extractions of the effective pomeron intercept describing the $x_{\mathbb{P}}$ dependence of diffractive DIS data at different Q^2 values.

To good approximation, LRG and LPS data show that diffractive DIS data satisfy a proton vertex factorization, whereby the dependences on variables which describe the scattered proton ($x_{\mathbb{P}}$, t) factorize from those describing the hard partonic interaction (Q^2 , β). For example, the slope parameter b , extracted by fitting the t distribution

to the form $d\sigma/dt \propto e^{bt}$, is shown as a function of diffractive DIS (DDIS) kinematic variables in Fig. 5.a. There are no significant variations from the average value of $b \simeq 7$ GeV $^{-2}$ anywhere in the studied range. The measured value of b is significantly larger than that from ‘hard’ exclusive vector meson production ($ep \rightarrow eVp$). It is characteristic of an interaction region of spatial extent considerably larger than the proton radius, indicating that the dominant feature of DDIS is the probing with the virtual photon of non-perturbative exchanges similar to the Pomeron of soft hadronic physics.

Fig. 5.b shows the Q^2 dependence of the effective Pomeron intercept $\alpha_{\mathbb{P}}(0)$, which is extracted from the $x_{\mathbb{P}}$ dependence of the data. No significant dependence on Q^2 is observed, again compatible with proton vertex factorization.

The intercept of the effective Pomeron trajectory is consistent within errors with the soft Pomeron results from fits to total cross sections and soft diffractive data. Although larger effective intercepts have been measured in hard vector meson production, no deviations with either Q^2 or β have yet been observed in inclusive diffractive DIS.

3. Diffractive PDFs at HERA

In order to compare diffractive data with perturbative QCD models, or parton-driven models, the first step is to show that the diffractive cross section shows a hard dependence in the center-of-mass energy W of the γ^*p system. In Fig. 6., we observe a behavior of the form $\sim W^{0.6}$, compatible with the dependence expected for a hard process. This observation is obviously the key to allow further studies of the diffractive process in the context of perturbative QCD [3]. Events with the diffractive topology can be studied in terms of Pomeron trajectory exchanged between the proton and the virtual photon. In this view, these events result from a color-singlet exchange between the diffractively dissociated virtual photon and the proton (see Fig. 7.).

A diffractive structure function $F_2^{D(3)}$ can then be defined as a sum of two factorized contributions, corresponding to a Pomeron and secondary Reggeon trajectories:

$$F_2^{D(3)}(Q^2, \beta, x_{\mathbb{P}}) = f_{\mathbb{P}/p}(x_{\mathbb{P}})F_2^{D(\mathbb{P})}(Q^2, \beta) + f_{\mathbb{R}/p}(x_{\mathbb{P}})F_2^{D(\mathbb{R})}(Q^2, \beta),$$

where $f_{\mathbb{P}/p}(x_{\mathbb{P}})$ is the Pomeron flux. It depends only on $x_{\mathbb{P}}$, once integrated over t , and $F_2^{D(\mathbb{P})}$ can be interpreted as the Pomeron structure function, depending on β and Q^2 . The other function, $F_2^{D(\mathbb{R})}$, is an effective Reggeon structure function taking into account various secondary Regge contributions which can not be separated. The Pomeron and Reggeon fluxes are assumed to follow a Regge behavior with linear trajectories $\alpha_{\mathbb{P},\mathbb{R}}(t) = \alpha_{\mathbb{P},\mathbb{R}}(0) + \alpha'_{\mathbb{P},\mathbb{R}}t$, such that

$$f_{\mathbb{P}/p,\mathbb{R}/p}(x_{\mathbb{P}}) = \int_{t_{cut}}^{t_{min}} \frac{e^{B_{\mathbb{P},\mathbb{R}}t}}{x_{\mathbb{P}}^{2\alpha_{\mathbb{P},\mathbb{R}}(t)-1}} dt, \quad (1)$$

where $|t_{min}|$ is the minimum kinematically allowed value of $|t|$ and $t_{cut} = -1$ GeV 2 is the limit of the measurement. We take $\alpha'_{\mathbb{P}} = 0.06$ GeV $^{-2}$, $\alpha'_{\mathbb{R}} = 0.30$ GeV $^{-2}$, $B_{\mathbb{P}} = 5.5$ GeV $^{-2}$ and $B_{\mathbb{R}} = 1.6$ GeV $^{-2}$. The Pomeron intercept $\alpha_{\mathbb{P}}(0)$ is left as a free parameter in the QCD fit and $\alpha_{\mathbb{R}}(0)$ is fixed to 0.50.

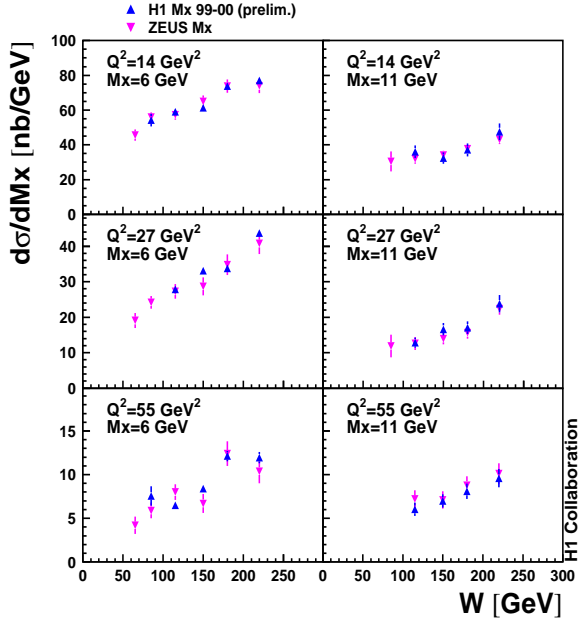


Fig. 6. Cross sections of the diffractive process $\gamma^*p \rightarrow p'X$, differential in the mass of the diffractively produced hadronic system X (M_X), are presented as a function of the center-of-mass energy of the γ^*p system W . Measurements at different values of the virtuality Q^2 of the exchanged photon are displayed. We observe a behavior of the form $\sim W^{0.6}$ for the diffractive cross section, compatible with the dependence expected for a hard process.

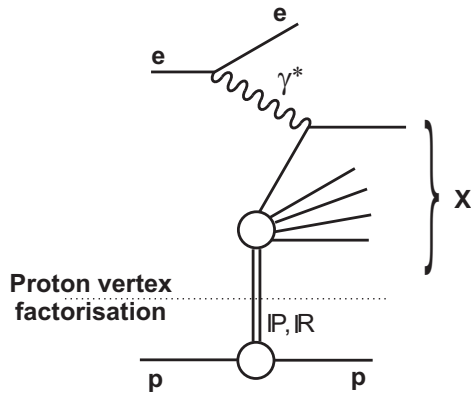


Fig. 7. Schematic diagram of a diffractive process. Events with a diffractive topology can be studied in terms of the Pomeron trajectory exchanged between the proton and the virtual photon.

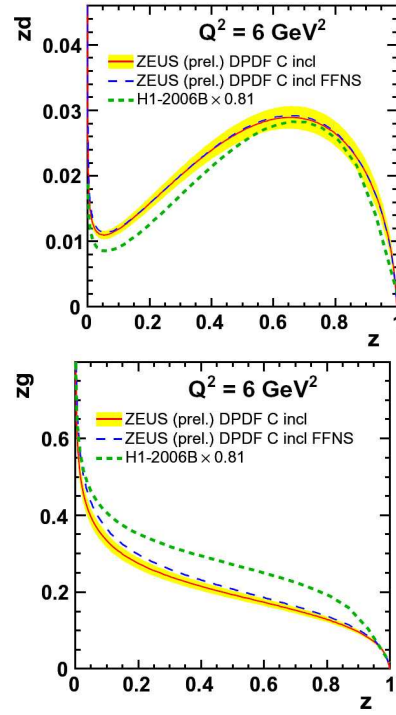


Fig. 8. ZEUS down quark (one sixth of the total quark + antiquark) and gluon densities as a function of generalised momentum fraction z at $Q^2 = 6 \text{ GeV}^2$ [6]. Two heavy flavour schemes are shown, as well as H1 results corrected for proton dissociation with a factor of 0.81.

The next step is then to model the Pomeron structure function $F_2^{D(P)}$ [1, 5, 6]. Among the most popular models, the one based on a point-like structure of the Pomeron has been studied extensively using a non-perturbative input supplemented by a perturbative QCD evolution equations [5, 6]. In this formulation, it is assumed that the exchanged object, the Pomeron, is a color-singlet quasi-particle whose structure is probed in the DIS process. As for standard DIS, diffractive parton distributions related to the Pomeron can be derived from QCD fits to diffractive cross sections. The procedure is standard: we assign parton distribution functions to the Pomeron parametrized in terms of non-perturbative input distributions at some low scale Q_0^2 . The quark flavor singlet distribution ($zS(z, Q^2) = u + \bar{u} + d + \bar{d} + s + \bar{s}$) and the gluon distribution ($zG(z, Q^2)$) are parametrized at this initial scale Q_0^2 , where $z = x_{i/P}$ is the fractional momentum of the Pomeron carried by the struck parton. Functions zS and zG are evolved to higher Q^2 using the next-to-leading order DGLAP evolution equations. For the structure of the sub-leading Reggeon trajectory, the pion structure function [4] is assumed with a free global normalization to be determined by the data. Diffractive PDFs (DPDFs) extracted from H1 and ZEUS data are shown in Fig. 8. [1, 5, 6]. We observe that some differences in the data are reflected in the DPDFs, but some basic features are common for all data sets and the resulting DPDFs. Firstly, the gluon density is larger than the sea quark density, which means that the major fraction of the momentum (about 70%) is carried by the gluon for a typical value of $Q^2 = 10 \text{ GeV}^2$. Secondly, we observe that the gluon density is quite large at large β , with a large uncertainty, which means that we expect positive scaling violations still at large values of β . This

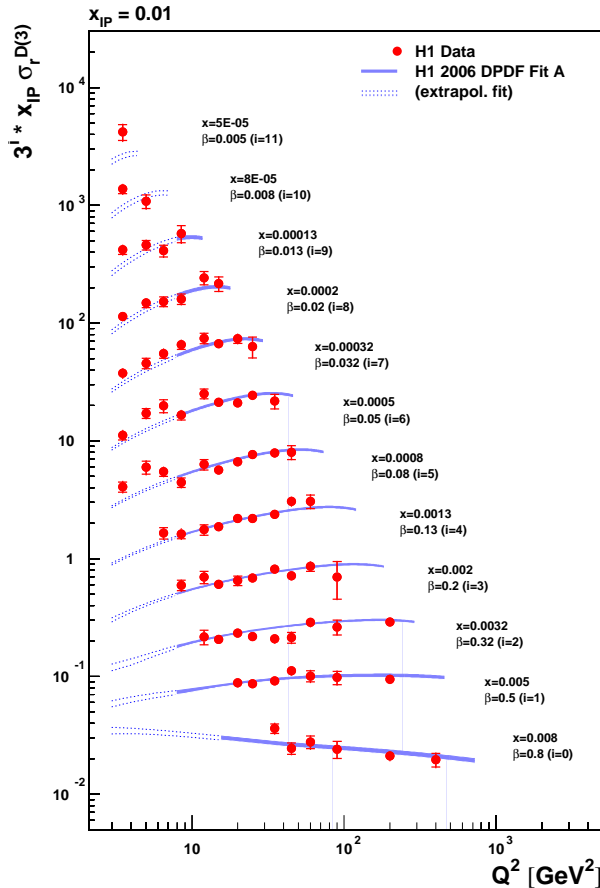


Fig. 9. Scaling violations for H1 diffractive cross sections for one value of x_P ($x_P = 0.01$) and a large range of β values, from low (< 0.01) to large values (> 0.5).

is shown in Fig. 9.. We note that even at large values of $\beta \sim 0.5$, the scaling violations are still positive, as discussed above. The strength of the DPDFs approach is to give a natural interpretation of this basic observation and to describe properly the Q^2 evolution of the cross sections. Other approaches are also well designed to describe all features of the data [8], but this is another story. The near future of the study of DPDFs is to combine all existing data and check their compatibility with respect to the QCD fit technique. If this is verified, a new global analysis can be followed to get the most complete understanding of DPDFs [5].

4. DPDFs and implications for the LHC

Note that diffractive distributions are process-independent functions. They appear not only in inclusive diffraction but also in other processes where diffractive hard-scattering factorization holds. The cross section of such a process can be evaluated as the convolution of the relevant parton-level cross section with the diffractive PDFs (DPDFs). For instance, the cross section for charm production in diffractive DIS can be calculated at leading order in α_s from the $\gamma^* g \rightarrow c\bar{c}$ cross section and the diffractive gluon distribution. An analogous statement holds for jet production in diffractive DIS. Both processes have been analyzed at next-to-leading order in α_s and are found to be consistent with the factorization theorem [3].

A natural question to ask is whether one can use the DPDFs extracted at HERA to describe hard diffractive processes such as the production of jets, heavy quarks

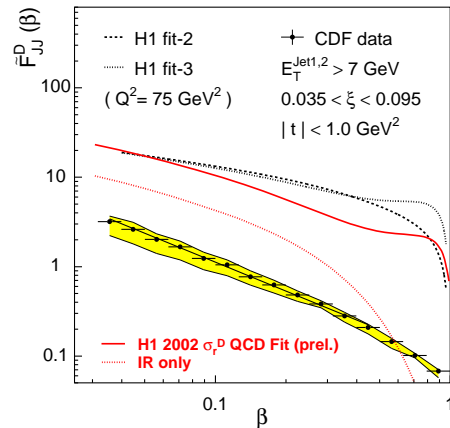


Fig. 10. Comparison between the CDF measurement of diffractive structure function (black points) with the H1 diffractive PDFs.

or weak gauge bosons in $p\bar{p}$ collisions at the Tevatron. Fig. 10. shows results on diffractive dijet production from the CDF collaboration compared to the expectations based on the DPDFs from HERA [7]. The discrepancy is spectacular: the fraction of diffractive dijet events at CDF is a factor 3 to 10 smaller than would be expected on the basis of the HERA data. The same type of discrepancy is consistently observed in all hard diffractive processes in $p\bar{p}$ events. In general, while at HERA hard diffraction contributes a fraction of order 10% to the total cross section, it contributes only about 1% at the Tevatron. This observation of QCD-factorization breaking in hadron-hadron scattering can be interpreted as a survival gap probability or a soft color interaction which needs to be considered in such reactions. In fact, from a fundamental point of view, diffractive hard-scattering factorization does not apply to hadron-hadron collisions. Attempts to establish corresponding factorization theorems fail, because of interactions between spectator partons of the colliding hadrons. The contribution of these interactions to the cross section does not decrease with the hard scale. Since they are not associated with the hard-scattering subprocess, we no longer have factorization into a parton-level cross section and the parton densities of one of the colliding hadrons. These interactions are generally soft, and we have at present to rely on phenomenological models to quantify their effects [7]. The yield of diffractive events in hadron-hadron collisions is then lowered precisely because of these soft interactions between spectator partons (often referred to as re-interactions or multiple scatterings). They can produce additional final-state particles which fill the would-be rapidity gap (hence the often-used term rapidity gap survival). When such additional particles are produced, a very fast proton can no longer appear in the final state because of energy conservation. Diffractive factorization breaking is thus intimately related to multiple scattering in hadron-hadron collisions. Understanding and describing this phenomenon is a challenge in the high-energy regime that will be reached at the LHC [9]. We can also remark simply that the collision partners, in pp or $p\bar{p}$ reactions, are both composite systems of large transverse size, and it is not too surprising that multiple interactions between their constituents can be substantial. In contrast, the virtual photon in γ^*p collisions has small transverse size, which disfavors multiple interactions and enables diffractive factorization to hold. According to

our discussion, we may expect that for decreasing virtuality Q^2 the photon behaves more and more like a hadron, and diffractive factorization may again be broken.

5. A brief comment on unitarity and diffraction

Kaidalov et al. [10] have investigated what fraction of the gluon distribution in the proton leads to diffractive final states. The ratio of diffractive to inclusive dijet production cross sections as a function of x_{Bj} of the gluon, for different hard scattering scales and for the diffractive PDFs is presented in Fig. 11.. This ratio should

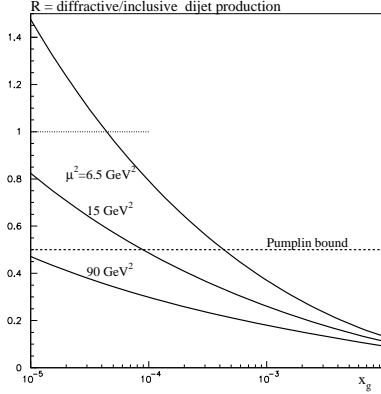


Fig. 11. The ratio of diffractive to inclusive dijet production cross section as a function of x_{Bj} of the gluon for different scales of the hard scattering, for the diffractive PDFs. Also shown is the unitarity limit, called Pumpkin bound.

be smaller than 0.5 [11], while for scales $\mu^2 = 15 \text{ GeV}^2$ this limit is exceeded for $x = 10^{-4}$. This indicates that unitarity effects may already be present in diffractive scattering.

6. The dipole picture of hadronic diffraction

The dynamics behind diffractive DIS can be easier understood if the process is viewed in the rest frame of the proton. The virtual photon develops a partonic fluctuations, whose lifetime is $\tau = 1/2m_p x$ [12]. At the small x_{Bj} typical of HERA, where $\tau \sim 10 - 100 \text{ fm}$, it is the partonic state rather than the photon that scatters off the proton (see Fig. 12.). If the scattering is elastic, the final state will have the features of diffraction.

The fluctuations of the γ^* are described by the wave functions of the transversely and longitudinally polarized γ^* which are known from perturbative QCD. Small and large partonic configurations of the photon fluctuation are present. For large configurations non-perturbative effects dominate in the interaction and the treatment of this contribution is subject to modeling. For a small configuration of partons (large relative k_T) the total interaction cross section of the created color dipole on a proton target can be expressed as

$$\sigma_{q\bar{q}p} = \frac{\pi^2}{3} r^2 \alpha_S(\mu) x g(x, \mu), \quad (2)$$

$$\sigma_{q\bar{q}gp} \simeq \sigma_{ggp} = \frac{9}{4} \sigma_{q\bar{q}p}, \quad (3)$$

where r is the transverse size of the color dipole and $\mu \sim 1/r^2$ is the scale at which the gluon distribution g of the proton is probed. The corresponding elastic cross section is obtained from the optical theorem. In this picture, the gluon dominance in diffraction results from the dynamics of perturbative QCD (see equation (3)) [13].

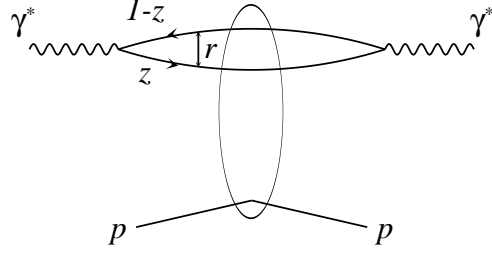


Fig. 12. Picture for the total cross section ($\gamma^* p \rightarrow \gamma^* p$) in the dipole model.

Models of diffraction that follow this approach are quite successful in describing both the inclusive F_2 and the diffractive F_2^D measurements, where the former are used to parameterize the dipole-proton cross section [13].

7. Exclusive processes in DIS

The presence of small size $q\bar{q}$ configurations in the photon can be tested in exclusive vector meson (VM) production as well as for deeply inelastic Compton scattering. At high energy (low x_{Bj}) and in the presence of a large scale (large Q^2 or heavy flavor), these reactions are expected to be driven by two-gluon exchange.

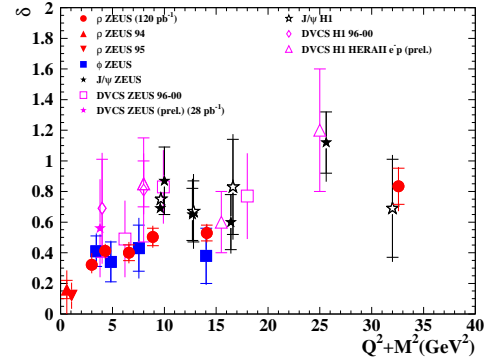


Fig. 13. Logarithmic derivatives $\delta = d \log \sigma(\gamma^* p) / d \log W$ as a function of $Q^2 + M_V^2$ for exclusive VM production.

A closer look at the theory of exclusive processes in QCD shows that the two partons taking part in the exchange do not carry the same fraction of the proton momentum. That makes these processes sensitive to correlations between partons, which are encoded in the so-called generalized parton distributions, GPDs [14]. These new functions relate in various limits to the parton distributions, form factors and orbital angular momentum distributions. The motivation behind studies of exclusive processes is to establish the region of validity of pQCD expectations and ultimately to pursue a full mapping of the proton structure, which cannot be achieved in inclusive measurements [15].

The cross section for the exclusive processes is expected to rise with W , with the rate of growth increasing with the value of the hard scale. A compilation of logarithmic derivatives $\delta = d \log \sigma(\gamma^* p) / d \log W$, for ρ , ϕ and J/ψ exclusive production, as a function of the scale defined as $Q^2 + M_V^2$, where M_V is the mass of the VM, is presented in Fig. 13. [15].

In Fig. 13., we observe a universal behavior, showing an increase of δ as the scale becomes larger. The value of δ at low scale is the one expected from the soft Pomeron

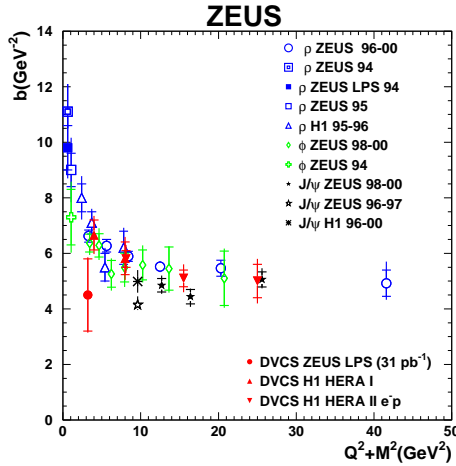


Fig. 14. Exponential slope of the t distribution measured for exclusive VM production as a function of $Q^2 + M_V^2$.

intercept, while the one at large scale is in accordance with twice the logarithmic derivative of the gluon density with respect to W . Then, when δ is measured to be of the order of 0.6 or higher, the process is hard and calculable in perturbative QCD.

Another fundamental measurement concerns the cross section of exclusive VM production, differential in t , where $t = (p - p')^2$ is the momentum transfer (squared) at the proton vertex. A parametrization in $d\sigma/dt \sim e^{-b|t|}$ gives a very good description of all measurements in the kinematic range of HERA (at low $x < 0.01$). Then, when $Q^2 + M_V^2$ is increasing, which corresponds to a decreasing transverse size of the $q\bar{q}$ dipole, the t distribution is expected to become universal, independent of the scale and of the VM. The exponential slope of the t distribution, b , reflects then the size of the proton. A compilation of measured b values is presented in Fig. 14.. Around $Q^2 + M_V^2$ of about 15 GeV^2 indeed the b values become universal. A qualitative understanding of this behavior is simple. Indeed, b is essentially the sum of a component coming from the probe in $1/\sqrt{Q^2 + M_{VM}^2}$ and a component related to the target nucleon. Then, at large Q^2 or large M_{VM}^2 , the b values decrease to the solely target component. That's why in Fig. 14., we observe that for large Q^2 or for heavy VMs, like J/ψ , b is reaching a universal value of about 5 GeV^{-2} , scaling with Q^2 asymptotically. This value is related to the size of the target probed during the interaction and we do not expect further decrease of b when increasing the scale, once a certain scale is reached [15].

8. Nucleon Tomography

Measurements of the t -slope parameters b , presented in the previous section (Fig. 14.), are key measurements for almost all exclusive processes. Indeed, a Fourier transform from momentum to impact parameter space readily shows that the t -slope b is related to the typical transverse distance between the colliding objects. At high scale, the $q\bar{q}$ dipole is almost point-like, and the t dependence of the cross section is given by the transverse extension of the gluons (or sea quarks) in the proton for a given x_{Bj} range. In particular for DVCS [16], interpretation of t -slope measurements does not suffer from the lack of knowledge of the VM wave function. Then, a

DVCS cross section, differential in t , is directly related to GPDs [14]. More precisely, from GPDs, we can compute a parton density which also depends on a spatial degree of freedom, the transverse size (or impact parameter), labeled R_\perp , in the proton. Both functions are related by a Fourier transform

$$PDF(x, R_\perp; Q^2) \equiv$$

$$\int \frac{d^2\Delta_\perp}{(2\pi)^2} e^{i(\Delta_\perp R_\perp)} GPD(x, t = -\Delta_\perp^2; Q^2).$$

Thus, the transverse extension $\langle r_T^2 \rangle$ of gluons (or sea quarks) in the proton can be written as

$$\begin{aligned} \langle r_T^2 \rangle &\equiv \frac{\int d^2R_\perp PDF(x, R_\perp) R_\perp^2}{\int d^2R_\perp PDF(x, R_\perp)} \\ &= 4 \frac{\partial}{\partial t} \left[\frac{GPD(x, t)}{GPD(x, 0)} \right]_{t=0} = 2b \end{aligned}$$

where b is the exponential t -slope. Measurements of b presented in Fig. 14. corresponds to $\sqrt{r_T^2} = 0.65 \pm 0.02$ fm at large scale Q^2 for $x_{Bj} < 10^{-2}$. This value is smaller than the size of a single proton, and, in contrast to hadron-hadron scattering, it does not expand as energy W increases. This result is consistent with perturbative QCD calculations in terms of a radiation cloud of gluons and quarks emitted around the incoming virtual photon. In short, gluons are located at the periphery of the proton as measured here and valence quarks are assumed to form the core of the proton at small value of $\sqrt{r_T^2}$.

In other words, the Fourier transform of the DVCS amplitude is the amplitude to find quarks at R_\perp in an image plane after focusing by an idealized lens. The square of the profile amplitude, producing the PDF (in transverse plane) is positive, real-valued, and corresponds to the image, a weighted probability to find quarks in the transverse image plane.

9. Perspectives at CERN

The complete parton imaging in the nucleon would need to get measurements of b for several values of x_{Bj} , from the low $x_{Bj} < 0.01$ till $x_{Bj} > 0.1$. Experimentally, it appears to be impossible. Is it the breakout of quark and gluon imaging in the proton? In fact, there is one way to recover x_{Bj} and t correlations over the whole x_{Bj} domain: we need to measure a Beam Charge Asymmetry (BCA).

A determination of a cross section asymmetry with respect to the beam charge has been realized by the H1 experiment by measuring the ratio $(d\sigma^+ - d\sigma^-)/(d\sigma^+ + d\sigma^-)$ as a function of ϕ , where ϕ is the azimuthal angle between leptons and proton plane. The result has recently been obtained by the H1 collaboration (see Ref. [16]) with a fit in $\cos\phi$. After applying a deconvolution method to account for the resolution on ϕ , the coefficient of the $\cos\phi$ dependence is found to be $p_1 = 0.16 \pm 0.04(\text{stat.}) \pm 0.06(\text{sys.})$. This result represents obviously a major progress in the understanding of the very recent field of the parton imaging in the proton. We are at the hedge of the giving a new reading on the most fundamental question to know how the proton is built up by quarks and gluons.

Feasibilities for future BCA measurements at COMPASS have been studied extensively in the last decade [17]. COMPASS is a fixed target experiment which can use 100 GeV muon beams and hydrogen targets, and

then access experimentally the DVCS process $\mu p \rightarrow \mu \gamma p$. The BCA can be determined when using positive and negative muon beams. One major interest is the kinematic coverage from 2 GeV² till 6 GeV² in Q^2 and x_{Bj} ranging from 0.05 till 0.1. It means that it is possible to avoid the kinematic domain dominated by higher-twists and non-perturbative effects (for $Q^2 < 1$ GeV²) and keeping a x_{Bj} range which is extending the HERA (H1/ZEUS) domain.

10. Conclusions

We have reviewed the most recent experimental results from hard diffractive scattering at HERA and Tevatron. We have shown that many aspects of diffraction in ep collisions can be successfully described in QCD if a hard scale is present. A key to this success are factorization theorems, which render parts of the dynamics accessible to calculation in perturbation theory. The remaining non-perturbative quantities, namely diffractive PDFs and generalized parton distributions, can be extracted from measurements and contain specific information about small- x_{Bj} partons in the proton that can only be obtained in diffractive processes. To describe hard diffractive hadron-hadron collisions is more challenging since factorization is broken by re-scattering between spectator partons. These re-scattering effects are of interest in their own right because of their intimate relation with multiple scattering effects, which at LHC energies are expected to be crucial for understanding the structure of events in hard collisions.

A combination of data on inclusive and diffractive ep scattering hints at the onset of parton saturation at HERA, and the phenomenology developed there is a helpful step towards understanding high-density effects in hadron-hadron collisions. In this respect, we have discussed a very important aspect that makes diffraction in DIS so interesting at low x_{Bj} . Its interpretation in the dipole formalism and its connection to saturation effects. Indeed, diffraction in DIS has appeared as a well suited process to analyze saturation effects at large gluon density in the proton. In the dipole model, it takes a simple and luminous form, with the introduction of the so-called saturation scale Q_s . Diffraction is then dominated by dipoles of size $r \sim 1/Q_s$. In particular, it provides a simple explanation of the constance of the ratio of diffractive to total cross sections as a function of W (at fixed Q^2 values).

Then, exclusive processes in DIS, like VMs production or DVCS, have appeared as key reactions to trigger the generic mechanism of diffractive scattering. Decisive measurements have been performed recently, in particular concerning dependences of exclusive processes cross section within the momentum exchange (squared) at the proton vertex, t . This allows to extract first experimental features concerning proton tomography, on how partons are localized in the proton. It provides a completely new information on the spatial extension of partons inside the proton (or more generally hadrons), as well as on the correlations of longitudinal momenta. A unified picture of this physics is encoded in the GPDs formalism. We have shown that Jefferson laboratory experiments or prospects at COMPASS are essential, to gain relevant information on GPDs. Of course, we do not forget that the dependence of GPDs on three kinematical variables, and the number of distributions describing different helicity combinations present a considerable complexity. In a sense this is the price to pay for the amount of physics information encoded in these quantities. It is however crucial to realize that for many important aspects we need not fully disentangle this complexity. The relation of longitudinal and transverse structure of partons in

a nucleon, or of nucleons in a nucleus, can be studied quantitatively from the distribution in the two external kinematical variables x_{Bj} and t .

References

- [1] A. Aktas *et al.* [H1 Collaboration], Eur. Phys. J. C **48** (2006) 715; Eur. Phys. J. C **48** (2006) 749; ZEUS Collab., S. Chekanov *et al.*, Nucl. Phys. B **713** (2005) 3; Eur. Phys. J. C **38** (2004) 43.
- [2] M. Ruspa *et al.* [ZEUS Collaboration], [arXiv:hep-ex/0808.0833].
- [3] J.C. Collins, Phys. Rev. D **57** (1998) 3051 [Erratum-ibid. D **61** (2000) 019902].
- [4] J.F. Owens, Phys. Rev. D **30** (1984) 943.
- [5] C. Royon, L. Schoeffel, S. Sapeta, R.B. Peschanski and E. Sauvan, Nucl. Phys. B **781** (2007) 1; C. Royon, L. Schoeffel, R.B. Peschanski and E. Sauvan, Nucl. Phys. B **746** (2006) 15; C. Royon, L. Schoeffel, J. Bartels, H. Jung and R. B. Peschanski, Phys. Rev. D **63** (2001) 074004.
- [6] ZEUS Collaboration, ‘A QCD analysis of diffractive DIS data from ZEUS’ [ZEUS-pub-09-010].
- [7] T. Affolder *et al.* [CDF Collaboration], Phys. Rev. Lett. **84** (2000) 5043.
- [8] C. Marquet and L. Schoeffel, Phys. Lett. B **639** (2006) 471.
- [9] AFP TDR in ATLAS to be submitted; see: <http://project-rp220.web.cern.ch/project-rp220/index.html>.
- [10] A. B. Kaidalov, V. A. Khoze, A. D. Martin and M. G. Ryskin, Phys. Lett. B **567**, 61 (2003), hep-ph/0306134.
- [11] J. Pumplin, Phys. Rev. D **8** (1973) 2899.
- [12] B. L. Ioffe, V. A. Khoze and L. N. Lipatov, “Hard Processes. Vol. 1: Phenomenology, Quark Parton Model,” *Amsterdam, Netherlands: North-Holland, 1984*.
- [13] A.H. Mueller, Nucl. Phys. B **335** (1990) 115; N.N. Nikolaev and B.G. Zakharov, Zeit. für. Phys. C **49** (1991) 607; A. Bialas and R. Peschanski, Phys. Lett. B **378** (1996) 302; Phys. Lett. B **387** (1996) 405; H. Navelet, R. Peschanski, C. Royon, S. Wallon, Phys. Lett. B **385** (1996) 357; H. Navelet, R. Peschanski, C. Royon, Phys. Lett. B **366** (1996) 329; K. J. Golec-Biernat and M. Wusthoff, Phys. Rev. D **59** (1999) 014017; Phys. Rev. D **60** (1999) 114023; A. Bialas, R. Peschanski, C. Royon, Phys. Rev. D **57** (1998) 6899; S. Munier, R. Peschanski, C. Royon, Nucl. Phys. B **534** (1998) 297; E. Iancu, K. Itakura and S. Munier, Phys. Lett. B **590** (2004) 199.
- [14] M. Diehl, T. Gousset, B. Pire and J. P. Ralston, Phys. Lett. B **411** (1997) 193; L. L. Frankfurt, A. Freund and M. Strikman, Phys. Rev. D **58** (1998) 114001 [Erratum-ibid. D **59** (1999) 119901]; A. V. Belitsky, D. Mueller and A. Kirchner, Nucl. Phys. B **629** (2002) 323; M. Diehl, Phys. Rept. **388**, 41 (2003).
- [15] L. Schoeffel, arXiv:0908.3287 [hep-ph].
- [16] H. Collaboration, arXiv:0907.5289 [hep-ex]; Eur. Phys. J. C **44** (2005) 1; S. Chekanov *et al.* [ZEUS Collaboration], JHEP **0905** (2009) 108.
- [17] N. d’Hose *et al.*, Nucl. Phys. A **711** (2002) 160.